Mon. Not. R. Astron. Soc. **000**, 1–10 (2011) Printed 18 February 2022 (MN LATEX style file v2.2)

The missing link: a low mass X-ray binary in M31 seen as an ultraluminous X-ray source

Matthew J. Middleton, Andrew D. Sutton, Timothy P. Roberts, Floyd E. Jackson and Chris Done
Department of Physics, University of Durham, South Road, Durham DH1 3LE, UK

arXiv:1111.1188v1 [astro-ph.HE] 4 Nov 2011

18 February 2022

ABSTRACT

A new, transient ultraluminous X-ray source (ULX) was recently discovered by *Chandra* in M31 with a luminosity at $\sim 5{\times}10^{39}$ erg s^{-1}. Here we analyse a series of five subsequent *XMM-Newton* observations. These show a steady decline in X-ray luminosity over 1.5 months, from $1.8 - 0.6 \times 10^{39}$ erg s^{-1}, giving an observed e-fold timescale of ~ 40 days. This is similar to the decay timescales seen in multiple soft X-ray transients in our own Galaxy, supporting the interpretation of this ULX as a stellar mass black hole in a low-mass X-ray binary (LMXB), accreting at super Eddington rates. This is further supported by the lack of detection of an O/B star in quiescence and the spectral behaviour of the *XMM-Newton* data being dominated by a disc-like component rather than the power-law expected from a sub-Eddington intermediate-mass black hole.

These data give the best sequence of high Eddington fraction spectra ever assembled due to the combination of low absorption column to M31 and well calibrated bandpass down to 0.3 keV of *XMM-Newton* in full frame mode. The spectra can be roughly described by our best current disc model, BHSPEC, assuming a 10 $M_\odot$ black hole with best fit spin ~ 0.4, declining from $L/L_{Edd} = 0.75$–0.25. However, the data are better described by a two component model, where the disc emission is significantly affected by advection, and with an additional low temperature Comptonisation component at high energies which becomes more important at high luminosities. This could simply indicate the limitations of our current disc models, though changes in the energy-dependent variability also weakly supports a two component interpretation of the data.

Irrespective of the detailed interpretation of the spectral properties, these data support the presence of accretion onto a stellar mass black hole in a LMXB accreting in the Eddington-regime. This allows an unambiguous connection of this object, and, by extension, similar low luminosity ULXs, to 'standard' X-ray binaries.

Key words: accretion, accretion discs – X-rays: binaries, black hole

1 INTRODUCTION

The broad population of X-ray sources in our own Galaxy includes, amongst others, X-ray binaries (XRBs) believed to be powered by accretion of material onto a compact object, usually a neutron star or black hole (BH). These dominate the X-ray sky of the Galaxy and are important objects to study as they provide high quality data, allowing an insight into the nature of accretion. In the case of low-mass companion systems (LMXBs) the X-ray emission characteristics are well described by the presence of an optically thick, geometrically thin accretion disc (Shakura & Sunyaev 1973) and/or Comptonisation of the disc emission in a hot plasma (Titarchuk 1994). However, as the luminosity of these systems approaches their Eddington limit our understanding breaks down. Proposed models have included the production of large-scale winds driven by the large radiation pressure (Poutanen et al. 2007; Kajava & Poutanen 2009; King 2004) whilst others favour the disc structure becoming radiatively inefficient and instead dominated by optically thick advection processes (Abramowicz et al. 1988; Mineshige et al. 2000). Although a small number of XRBs have been inferred to accrete at these high rates (V404 Cyg: Życki,

© 2011 RAS

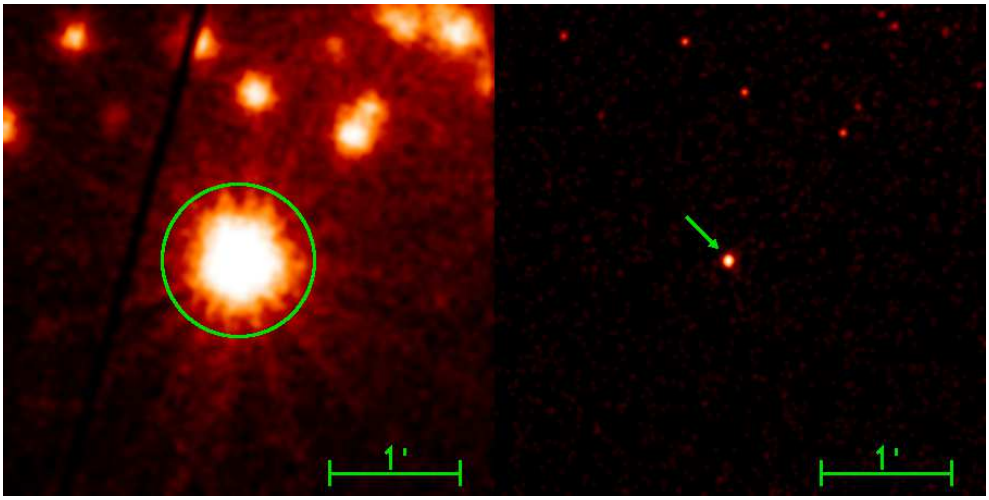


Figure 1. *Left: XMM-Newton* EPIC PN image of M31 ULX-1 with the 35" extraction region overlaid. *Right: Chandra* HRC-I image of the source taken eleven days earlier. Through performing relative astrometry between the *Chandra* and *XMM-Newton* fields, we are confident that these are images of the same source.

Done & Smith 1999; GRS 1915+105: McClintock & Remillard 2006; V4641: Revnivtsev et al. 2002; Cir X-1: Done & Gierliński 2003), the large intervening column of material within our own Galaxy prevents a detailed analysis of the behaviour of the disc. We cannot even look to the active centre of distant galaxies (AGN) for answers, as mass scaling places the disc emission firmly in the unobservable UV (although see Czerny et al. 2011; Done et al. 2011).

The proximity of our nearest neighbour galaxy, M31, has allowed the latest generation of observatories to detect (and often resolve) the X-ray bright menagerie of objects it plays host to. The range of objects in M31 is analogous to the population of X-ray sources we see in our own Galaxy (e.g. Pietsch et al. 2009). However, unlike our Galaxy, observations of the M31 population is not hindered by the large absorbing column of the Galactic disc (see Warwick et al. 2011) and the distance to the source has a much smaller relative uncertainty, improving the constraints on the X-ray luminosity.

One remarkable object in M31 has been seen to emit at very high luminosities based on the estimated distance of 0.7-0.8 Mpc (see Vilardell et al. 2010; Tanaka et al. 2010 etc.). CXOM31 J004253.1+411422 (M31 ULX-1 hereafter) was first detected by the high resolution camera (HRC-I) onboard NASA's *Chandra* mission at a count rate of 3.28 $\pm$ 0.04 ct s^{-1} (Henze et al. 2009, ATEL #2356). The follow-up *Swift* observation (OBSID 29762) placed a rough limit on the flux of the object in the *Chandra* observation at $\sim 5 \times 10^{39}$erg s^{-1}. Due to its luminosity ($> 10^{39}$erg s^{-1}) and distance from the centre of M31 (> 2'), this is a *bona fide* ultra-luminous X-ray source (ULX, see Roberts 2007). A sequence of several *XMM-Newton* observations, spaced at 7-10 day intervals, followed this bright detection and have captured the emission characteristics of the source over a period of $\sim$1 month (see also Kaur et al. 2011).

Assuming that the spectral behaviour is similar to that of other low-luminosity ULXs (e.g. Middleton, Sutton & Roberts 2011; Gladstone, Roberts & Done 2009; Weng et al. 2009; Dubus, Charles & Long 2004; La Parola et al. 2003; Parmar et al. 2001; Takano et al. 1994) then we expect there to be a significant disc blackbody component to the emission. Whilst ULXs are generally persistent in nature (although see e.g. Ghosh et al. 2006, Sivakoff et al. 2008), this object is clearly transient and, on this basis, has much more in common with the larger population of Galactic XRBs. These observations may therefore provide an unobscured description of accretion through a disc at high mass accretion rates. In this paper we will describe the temporal and spectral properties obtained from the high quality *XMM-Newton* data as the source dims from its peak observed brightness.

2 DATA ANALYSIS

In total, M31 ULX-1 has been observed 7 times in outburst; initially it was detected using the *Chandra* HRC-I, followed by a *Swift* target of opportunity (ToO) and then 5 *XMM-Newton* observations. The details of each of these are given in Table 1. To confirm that we are viewing the same object in all the observations we extracted the HRC-I data of the field when the source is bright (Fig. 1) and obtained the positions of all the point sources using CELLDETECT in CIAO v 4.1. We then used EDETECT in SAS v10 to obtain the analogous source positions in the EPIC PN field from the observation chronologically closest to the *Chandra* observation (OBSID 0600660201: Fig. 1). The positions of several bright sources common to both fields were then used to constrain their relative astrometry. The position of the ULX (as determined by the high resolution HRC-I of *Chandra*) at R.A.(J2000) = 00:42:53.15, Dec.(J2000) = +41:14:22.9 (with a typical error of $\sim$0.5") was consistent (within errors) in both fields, confirming it as a single transient object viewed at different epochs.

For each of the *XMM-Newton* detections we extracted the event files using SAS v10 and filtered the products for standard patterns (<=12 for MOS, <= 4 for PN) and flags (=0 for spectral and timing products). From these we ex-

Table 1. Observations of M31 ULX-1

Instrument	OBSID	obs. date	useful exposure (ks)	f_x ($\times 10^{-11}$ erg cm^{-2} s^{-1})	count rate (ct s^{-1})
Chandra HRC-I	10886	17-12-2009	19.0	6.40*	3.3
Swift XRT	29762	22-12-2009	4.4	2.40*	0.7
XMM-Newton EPIC	0600660201	28-12-2009	14.5	2.52	4.2
XMM-Newton EPIC	0600660301	07-01-2010	13.3	1.87	4.6
XMM-Newton EPIC	0600660401	15-01-2010	6.4	1.37	3.6
XMM-Newton EPIC	0600660501	25-01-2010	10.0	1.14	2.9
XMM-Newton EPIC	0600660601	02-02-2010	9.7	0.86	2.4

Notes: Observations of M31 ULX-1 by various missions over a period of $\sim$ 1.5 months. The useful exposure is the length of the observation following removal of background flares in the *Swift* XRT and *XMM-Newton* EPIC cameras (PN value given) respectively. f_x is the unabsorbed, integrated flux between 0.2–10 keV (from applying a simple continuum model to the data) and count rate is given for the PN in the *XMM-Newton* observations. Fluxes denoted by an asterisk (*) are taken from the literature values (Henze et al. 2009).

tracted spectral and timing properties from circular, 35" radius source and background regions from the same chip avoiding other sources in the field. We also filtered for hard (10–15 keV) background flaring intervals based on data from the entire chip, leaving the useful exposures given in Table 1.

In the first observation there was partial pile-up in the PN which we corrected for by removal of a 5" radius region around the centroid of the PSF, checking that the observed patterns were within the error bounds of the model patterns using the tool EPATPLOT. We found significant pile-up in the the first two MOS2 observations and, due to requiring large centroids for removal, we instead ignore these datasets.

We extracted spectral products using XSELECT, obtaining background-subtracted spectra and responses. We fit these using COMPTT to phenomenologically describe the continuum, with a neutral absorption column[1]. This describes the spectra well ($\chi^2 = 2809/2789$) for electron temperatures ranging from 0.94–0.78 keV, i.e. all spectra have a rollover well below 10 keV. We use this model to derive the unabsorbed 0.2–10 keV fluxes reported in Table 1.

We plot the unabsorbed flux as a function of time in Fig 2. There is a clear exponential decay, similar to that often seen in X-ray novae which can be modelled as $f(t) = f_0 \times e^{-t/\tau}$ where f is the flux after t days, f_0 is the initial flux and τ is the e-fold time. Given that the *Chandra* flux is only a rough estimate (Henze et al. 2009; ATEL #2356) we fit the full dataset (blue dashed line in Fig. 4) and the dataset without this point (red dot-dashed line) with a linear model in natural log space. These give e-fold times between 29 and 39 days respectively, consistent with that observed for X-ray novae in our own Galaxy (Shahbaz et al. 1998).

3 X-RAY SPECTRA

The *XMM-Newton* observations range from L_x=1.8-0.6$\times 10^{39}$ ergs s^{-1}, so only the first few datasets meet the ULX criteria of $>10^{39}$ ergs s^{-1}. These luminosities and heavily curved spectra (see previous section) clearly relate to standard stellar mass BHs accreting at close to the Eddington limit. The alternative explanation of an intermediate-mass BH (IMBH: Colbert & Mushotzky 1999), with 10^{2-5} M$_\odot$, would instead have $L/L_{Edd} \ll 0.1$ where the spectrum would be expected to be dominated by a hard power-law extending to $\sim$ 100 keV. This is plainly inconsistent with the observed rollover in the data below $\sim$10 keV. However, the *Chandra* discovery luminosity is $\sim 5\times 10^{39}$ ergs s^{-1}, so this source is clearly connected to the ULX regime.

Ruling out the presence of an IMBH means that the compact object driving the accretion is most likely a stellar mass BH. Assuming that the BH population is similar to that of our own Galaxy then we could be observing accretion onto a BH of mass $\sim$5–20 M$_\odot$ at rates of $L/L_{Edd} \sim 0.2 - 2$. XRBs accreting at similar rates have spectra which are dominated by a hot accretion disc, showing temperatures of $\sim$ 1 keV for luminosities up to Eddington (e.g. McClintock & Remillard 2006). In these disc dominated states, the maximum disc temperature and total luminosity change together such that $L \propto T^4$, indicating a constant inner emitting area, as predicted by the existence of the innermost stable circular orbit in general relativity (see e.g. Done, Gierliński & Kubota 2007).

3.1 Disc models

The most accurate available model for disc emission is BHSPEC (Davis et al. 2005) which self-consistently determines the spectrum at each radius by solving the vertical radiative transfer, and propagates this to the observer through the full general relativistic spacetime. These spectra are integrated over the entire disc, assuming the stress free inner boundary condition, with innermost radius fixed to the innermost stable circular orbit.

We fit this together with neutral absorption[1] to all the PN data across all of the observations simultaneously (we do not use the MOS datasets due to pile-up issues and the low effective area at high energies relative to the PN), fixing the inner radius of the disc (set by the BH spin) and inclination to be the same in all the datasets. As this source looks similar to many soft X-ray transients in our own Galaxy, we first

[1] with a lower limit based on the Galactic line-of-sight to M31 of $\sim 6.7\times 10^{20}$cm^{-2} (Dickey & Lockman 1990)

Table 2. Best fitting spectral parameters.

Observation	1	2	3	4	5
		TBABS*BHSPEC			
		$n_{\rm H} = 0.067\times10^{22}{\rm cm}^{-2}$			
		$\cos(i^\circ) = 0.87\ ^{+0.04}_{-0.02}$			
		$a_* = 0.36\ ^{+0.10}_{-0.11}$			
		BH mass ($M_\odot$) = 10*			
log $L/L_{\rm Edd}$	-0.133 $^{+0.016}_{-0.026}$	-0.283 $^{+0.015}_{-0.011}$	-0.418 $^{+0.016}_{-0.013}$	-0.521 $^{+0.005}_{-0.005}$	-0.612 $^{+0.005}_{-0.005}$
		χ^2 (d.o.f.) 3169.4 (2801)			
		Null P 1×10^{-6}			
		$n_{\rm H} < 0.068\times10^{22}{\rm cm}^{-2}$			
		$\cos(i^\circ) = 0.86$*			
		$a_* >0.76$			
		BH mass ($M_\odot$) = 14.9 $^{+0.2}_{-0.8}$			
log $L/L_{\rm Edd}$	-0.257 $^{+0.015}_{-0.005}$	-0.403 $^{+0.016}_{-0.005}$	-0.537 $^{+0.016}_{-0.006}$	-0.640 $^{+0.016}_{-0.005}$	-0.731 $^{+0.016}_{-0.006}$
		χ^2 (d.o.f.) 3078.5 (2801)			
		Null P 2×10^{-4}			
		$n_{\rm H} = 0.067\times10^{22}{\rm cm}^{-2}$			
		$\cos(i^\circ) = 0.5$*			
		$a_* = 0.76\ ^{+0.01}_{-0.01}$			
		BH mass ($M_\odot$) >29.6			
log $L/L_{\rm Edd}$	-0.381 $^{+0.007}_{-0.003}$	-0.530 $^{+0.006}_{-0.003}$	-0.664 $^{+0.008}_{-0.005}$	-0.766 $^{+0.007}_{-0.005}$	-0.857 $^{+0.008}_{-0.005}$
		χ^2 (d.o.f.) 3009.5(2801)			
		Null P 0.003			
		TBABS*(DISKPBB+COMPTT)			
		$n_{\rm H}$ 0.104 $^{+0.001}_{-0.001}$ $\times10^{22}{\rm cm}^{-2}$			
$kT_{\rm in}$ (keV)	0.44 $^{+0.08}_{-0.08}$	0.51 $^{+0.01}_{-0.01}$	0.67 $^{+0.03}_{-0.03}$	0.80 $^{+0.03}_{-0.03}$	0.92 $^{+0.03}_{-0.03}$
p	0.60 $^{+0.03}_{-0.01}$	0.60 $^{+0.03}_{-0.02}$	0.60 $^{+0.02}_{-0.01}$	0.56 $^{+0.01}_{-0.01}$	0.55 $^{+0.01}_{-0.01}$
$norm$	7.59	3.69	1.14	0.37	0.18
$kT_{\rm comp,seed}$ (keV)	0.55 $^{+0.10}_{-0.13}$	0.96 $^{+0.04}_{-0.04}$	0.61 $^{+0.27}_{-0.16}$	<1.26	——
$kT_{\rm comp}$ (keV)	0.98 $^{+0.30}_{-0.10}$	0.49 $^{+0.03}_{-0.02}$	0.81 $^{+0.06}_{-0.04}$	<11.73	——
τ	11.33 $^{+6.60}_{-5.22}$	16.39 $^{+4.09}_{-3.95}$	>19.00	(25.50)	——
		χ^2 (d.o.f.) 2752.2 (2777)			
		Null P 0.73			

Notes: BHSPEC model: best-fitting values of the Eddington fraction are given for spectral fitting, with fixed parameters denoted by *. We firstly fit the data with the mass fixed in the model at 10 $M_\odot$ (to be consistent with the BH population of our own Galaxy) with the inclination left free to vary, and subsequently with the inclination fixed at 30 and 60 degrees with BH mass free to vary. DISKPBB model: best fitting parameters are given for the 5 observations with the 5$^{\rm th}$ having no constrained Compton component in the spectrum. Where upper or lower limits are given, the lower (0.01 keV for the seed photon or electron temperature) or upper (200 for the optical depth, τ, 0.8 for the spin, a_* and 30 $M_\odot$ for the BH mass) hard boundaries for the model parameter have been reached. In the case of the optical depth for observation 4, the value is given in brackets as it is unconstrained. In all cases where there are two components, the degenerate nature of the spectral fitting requires one best-fitting component to be held in position whilst 90% error bounds are placed on the other. This is an unavoidable result of modelling such broad continua.

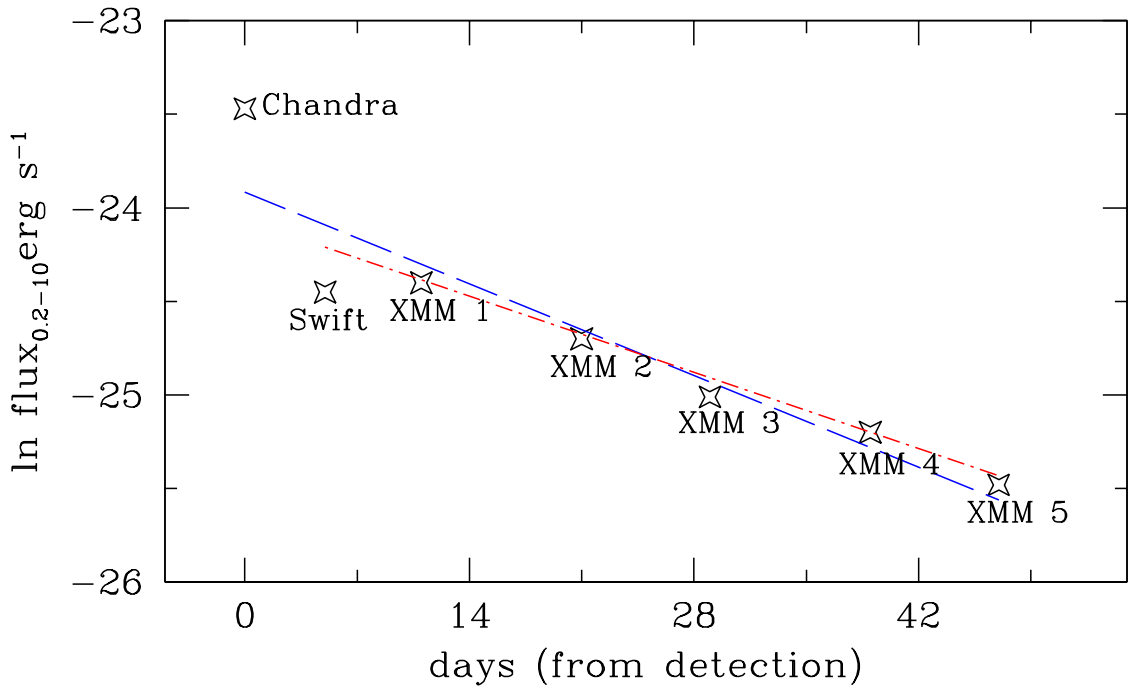


Figure 2. Unabsorbed 0.2–10 keV fluxes of M31 ULX-1 from observations taken with *Chandra*, *Swift* and *XMM-Newton* (see Table 1 for details of each of these). We fit the data with a ln-linearly decreasing trend and find that, by including the *Chandra* detection (blue dashed line), we obtain an *e*-fold time of 29 days and excluding it (red dot-dashed line), an *e*-fold time of 39 days. These derive from spline fitting in QDP and have variances of 0.36 and 0.03 with and without the Chandra flux point respectively. Both of these are consistent with the observed *e*-fold times of X-ray novae (e.g. Mineshige, Yamasaki & Ishizaka 1993).

assume a 10 $M_\odot$ BH. This gives a poor fit to the data (χ^2 = 3169/2801) while returning a reasonable value for the spin and inclination (see Table 2). However, we obtain a better fit by allowing the BH mass to be free. We tabulate results for $i = 30°$ and $60°$, with the latter giving the best fit (χ^2 = 3009/2801) and a BH mass pegged at the upper limit of 30 $M_\odot$. We show the data and residuals deconvolved with this best fit model in Figure 3.

The residuals indicate that the spectrum is somewhat broader than the disc models (resulting in the poor fit quality). This is commonly seen in *XMM-Newton* spectra of disc dominated XRBs (Kubota et al. 2010; Kolehmainen et al. 2011), but the level of residuals here is about twice as large. This could indicate that the wider bandpass used here (down to 0.3 keV rather than the 0.7 keV lower limit from the other CCD observations of disc dominated spectra) enhances the differences already seen between our best disc models and the data. Alternatively, the residuals could indicate that there is an additional component in the spectrum. XRBs commonly show a power-law tail to high energies, so we allow for this using the SIMPL model for Comptonisation (Steiner et al. 2009), fixing the power-law photon index to 2.2 as is commonly seen in the high/soft state (Kubota, Makishima & Ebisawa 2001). We include this additional component in our best fit model, but the improvement in χ^2 is not significant. The scattered fraction is always $\leq 5\%$, and the best fit disc parameters are not significantly different.

3.2 Disc plus low temperature Comptonisation

As the disc approaches the Eddington limit, optically thick advection should become important, where photons are swept along radially with the flow rather than escaping vertically (slim discs: Abramowicz et al. 1988). These photons can then be released in the plunging region where the flow becomes optically thin as it accelerates towards the event horizon (Sądowski 2009). Another process which can become important is a radiatively driven wind (Poutanen et al. 2007; Ohsuga & Mineshige 2011). At very high luminosities we expect the wind to launch at large radii in the disc, but at lower luminosities we may expect the wind to be launched only from the innermost radii of the disc where the radiation pressure is strongest. These processes are not mutually exclusive, and it seems most likely that both advection and wind-driving affect the spectra at Eddington and beyond (Ohsuga 2007; Ohsuga et al. 2009).

We have previously suggested that a wind-dominated model can explain both the spectral and timing characteristics of other ULXs at similar luminosities (Gladstone et al. 2009; Middleton et al. 2011b). The evolution of such systems is difficult to directly observe as most are persistent. However, in this case we see a clear drop in luminosity allowing the predictions of the model to be tested. In particular we expect that, as the mass accretion rate drops, the outer photospheric radius of the wind moves inwards as the radiation pressure decreases. The cool disc beyond the wind then has a smaller inner radius and should appear hotter. We describe this in XSPEC by a model comprising

a slim disc with the index of the temperature profile, p, a free parameter, together with thermal Comptonisation (with the seed temperature allowed to be free rather than being fixed to that of the disc) and neutral absorption[1] (in XSPEC: TBABS*(DISKPBB+COMPTT)). Although there is no real advantage to fitting the data simultaneously, we do so to allow a direct comparison with the disc-only model (BHSPEC).

The best-fitting model and associated residuals are shown together in Figure 3 (right hand panel) with the model components highlighted in Figure 4 and the parameters given in Table 2. We obtain an overall significant improvement in fit quality compared to the single disc model ($\Delta\chi^2$ of 257 for 24 extra d.o.f.). The best-fitting model parameters show that the temperature of the disc increases with decreasing luminosity, while its radius decreases. The corresponding Compton component peak temperature (which is a function of both seed photon temperature and electron temperature) also increases, but the fraction of the total luminosity carried by this drops with luminosity. This is broadly consistent with the predicted behaviour of a wind/photosphere launched from smaller radii as the radiation pressure drops (Middleton et al. 2011b). A possible issue arises where the disc at the lowest observed luminosity appears heavily advection dominated which is inconsistent with the inferred sub-Eddington mass accretion rate. Part of this is due to the lack of relativistic smearing in this model which makes the disc emission artificially narrow (Kolehmainen et al. 2011; Kubota et al. 2010).

We can obtain a rough estimate for the inner radius of the disc from the normalisation of the DISKPBB model. This drops from an apparent radius of 300 to 47 km assuming an inclination of 60°, which corresponds to a true inner radius of ∼400 to 62 km after correcting for colour temperature and stress free inner boundary condition (Kubota et al. 2001). The lowest number is similar to that derived from the BHSPEC fits for a 10 $M_\odot$ BH i.e. 71 km for $a = 0.36$, whereas the larger radii seen for the disc at higher luminosities in this model imply that the wind photosphere dominates down to $26R_g$. This is somewhat larger than expected given that a 10 $M_\odot$ BH is still sub-Eddington at this point, so should not yet power a strong wind. This would argue for a smaller mass BH (e.g. XTE J1650-500, Orosz et al. 2004), in order that the first few observations are super-Eddington.

4 SHORT TIMESCALE VARIABILITY

The spectra alone are somewhat degenerate. As we have shown, a description using only a single disc component (with fixed inner radius as the luminosity declines) is statistically poor. However, the best available models are not sufficiently well calibrated with the expectation of residuals when compared to the data. An alternative (and statistically better) description is a two component model, with an advective slim disc at low energies, together with an inner-disc wind photosphere at high energies which decreases in radius as the luminosity declines. We now use the additional information contained in the lightcurves to try to discriminate between these two very different interpretations of the spectra.

We can examine the variability as a function of energy within a given observation in several ways. The simplest of these is to obtain the variance of a light curve in a given energy band, subtract the expected variance of the Poisson (white) noise and normalise by the mean count rate to get the fractional variability (excess variance, or rms, see Edelson et al. 2002, Vaughan et al. 2003). We split the bandpass into 4 separate energy bins, from 0.3–0.7, 0.7–1.4, 1.4–3.0 and 3.0–10.0 keV and create lightcurves in each energy range, binned on 300 s (to provide adequate statistics for such an analysis) from coadding the PN and MOS data (we note that, due to the lower quality statistics, the small amount of pile-up in the first two MOS2 datasets adds only a small constant offset to variability at hard energies and so will have negligible effect upon the result). These showed some weak evidence for variability. We then carefully iterated the binning across the energy bandpass whilst ensuring adequate statistics remained in each bin under investigation and were able to find at least one energy range for each observation in which variability was detected at more than 3σ. However, the upper limits on variability in the remaining energy bins are large.

We can improve the statistics by using the energy band in which the variability is detected as a reference lightcurve to calculate the fractional covariance i.e. the amount of variability in the other energy bands which is correlated with the detected variability (see Wilkinson & Uttley 2009). The resulting energy-dependent fractional covariance spectra are shown in Figure 5, where the reference band value (red point) is the fractional rms. We have attempted to obtain as many constrained bins as possible, however, the lack of correlated variability makes this extremely difficult leaving us with only a small number of bins in each observation. Irrespective of this we can quite clearly see that the reference bandpass has the highest variability (by design), and that there is significantly less correlated variability at other energies in observations 1, 4 and 5. Additionally, the typical energy at which this variability is seen increases as the source declines. We note that observation 2 does not necessarily show a lack of correlated variability as the only other well constrained bin of excess variance (besides the reference band) is consistent within 1 sigma with the reference band whilst the nature of variability in observation 3 is difficult to accurately and reliably constrain due to the relative lack of counts above 2 keV.

We accept that it is possible that our iterative energy binning scheme could distort the statistical significance of this. Indeed, testing this approach on a similarly bright but constant source with similar observation length (G21.5-09, OBSID: 0122700101) can produce a single narrow bin of variability due to the inherent stochasticity of the white noise. However, it is highly unlikely that such a process could produce the observed energy dependence with luminosity seen in M31 ULX-1 and so we claim that there is real variability present. This energy dependence is difficult to explain in the single disc model. A disc dominated *XMM-Newton* spectrum from LMC X-3 shows variability on the few percent level (Kolehmainen et al. 2011, in prep), but this is constant across the entire energy band. Instead, it is much easier to explain in the two component model, where the interface between the disc and wind picks out a distinct radius and hence temperature, and this temperature increases as the wind photosphere radius decreases during the decline (see Fig 4). The modulation could be due either

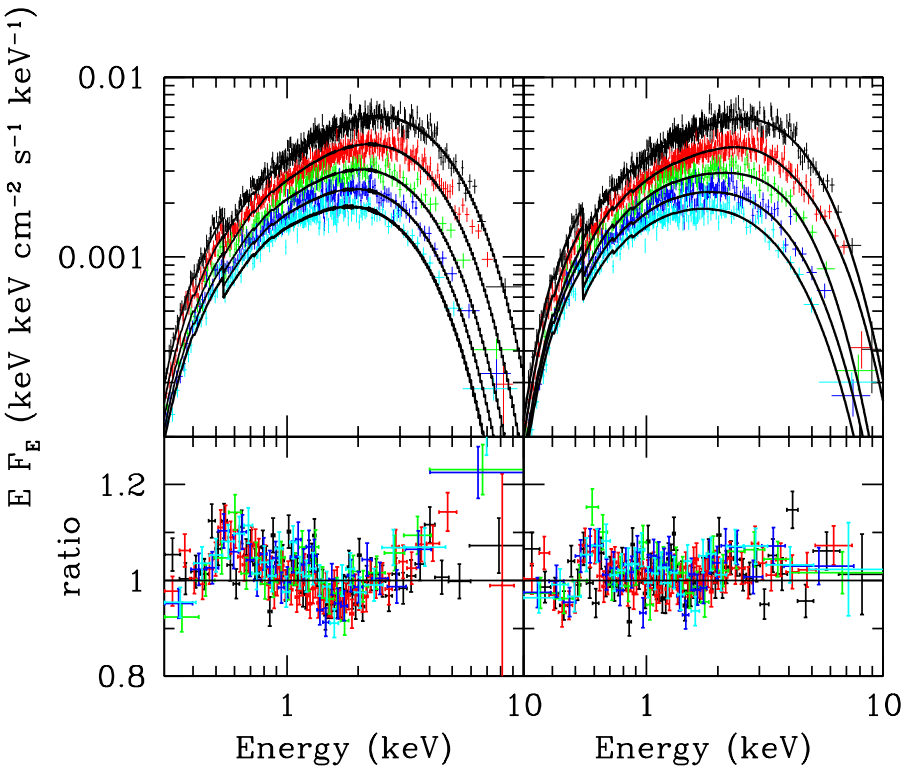


Figure 3. Simultaneous X-ray spectral fitting for M31 ULX-1 using the EPIC PN data across all 5 *XMM-Newton* observations (Obs1: black, Obs2: red, Obs3: green, Obs4: blue and Obs5: cyan). *Left*: we initially attempt to describe the data using a single disc model (BHSPEC). This can provide an acceptable fit quality but only for neutral absorption consistent with the Galactic column to M31. This model also suffers from systematically underestimating the flux at soft energies as can be seen in the ratio of data to the model (lower panel). This may indicate that the model is too simple, with the residuals potentially indicating emission from within the optically thin plunging region. *Right*: the same data but with a model of slim disc and inner photosphere/wind production. It is clear from inspecting the ratio to the best fitting model that the description is an improvement. This model can also describe the data for a larger absorption column (see Table 2).

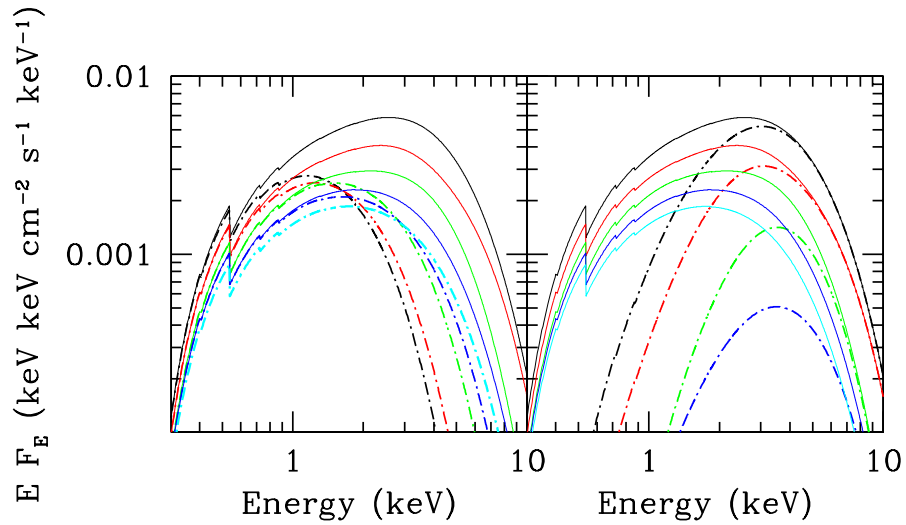


Figure 4. *Left*: Contribution of the disc component to the best fitting model of slim disk and photosphere/wind (the total model is given as a solid line and the disc component as a dot-dashed line with the colours corresponding to the observations in the caption of Fig. 2). As the source dims, the model predicts an increase in advection dominance and a broadening of the component. *Right*: The contribution to the same model from the photosphere/wind (dot-dashed line with colours as before). As the source dims, the model predicts that this component should get hotter and less dominant as it is driven from smaller, hotter radii.

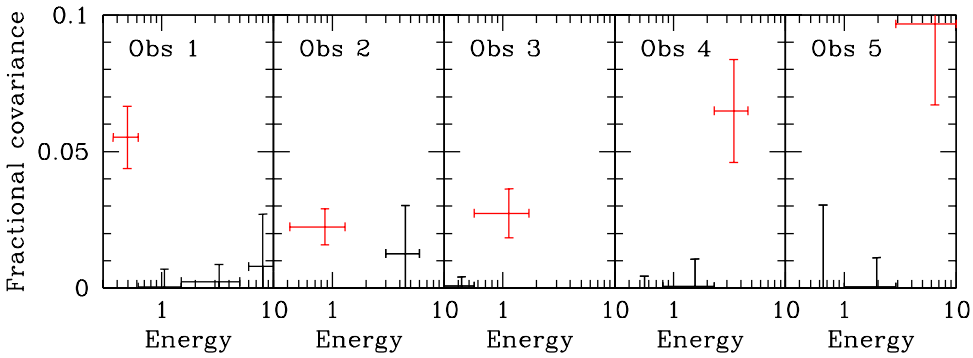


Figure 5. Fractional covariance for each of the observations on 300 s binning (to ensure adequate statistics) with the reference band shown in red (for which the value is the fractional excess variance). There is clearly a lack of evidence for correlated variability in any of the observations, whilst the well-constrained bin of variability is seen to increase in energy. This presents problems for our standard view of accretion disc behaviour but can be more readily explained by our ULX model.

to instabilities in the disc at this radius, or to the wind being clumpy and stochastically covering this inner region of the disc.

5 DISCUSSION & CONCLUSION

The combined spectral and timing behaviour of M31 ULX-1 allows a unique insight into the properties of a *bona fide* ULX, albeit a somewhat unusual ULX in being a transient rather than persistent system.

Garcia et al. (2010, ATEL #2474) determined the presence of an optical counterpart to the X-ray emission during the outburst, on the basis of a ~ 4 ks *HST* Advanced Camera for Surveys (ACS) F435W filter exposure taken on 2010 January 21, with an apparent magnitude of 23.8 (Figure 6, left hand panel). This is significantly brighter than a limit we derive from a later, post-outburst observation taken on 2010 July 20 in the same instrument, of $m_{\rm F435W} \approx 26$ (Figure 6, right hand panel). By converting the neutral absorption column measured from the X-ray data into an extinction using the relation of Predehl & Schmitt (1995), we find $A_B = 0.66$ towards the source in M31 (using the B filter as a close proxy of the *HST* F435W filter). We use this, and the magnitude limit, to derive an upper limit on the absolute magnitude of the optical counterpart in quiescence, presumably the emission of the secondary star in the system, of $M_{\rm F435W} \approx +1$. This rules out a high mass O or B star companion to the compact object, consistent with the identification of this transient as an LMXB. The lack of a persistent bright optical counterpart also implies that the detected transient optical emission is most likely from reprocessing in the X-ray illuminated outer disc (van Paradijs 1996).

The source lightcurve also strongly supports an LMXB identification (Fig 2). There is a clear, dramatic outburst, followed by an exponential decay. Such outbursts are triggered by the hydrogen ionisation instability in the outer disc, and so requires a low mass transfer rate from the companion star. A high mass companion filling its Roche lobe would have too large a mass transfer rate, making the system persistent rather than transient (King 1999).

The e-fold timescale of 39 days is also very similar to that seen in many stellar mass BH LMXB transients in our own Galaxy (Chen, Shrader & Livio 1997; Shabaz et al. 1998; Mineshige, Yamasaki & Ishizaka 1993). We can use this timescale to estimate the radius of the ionised disc (from equation 14 of Shahbaz, Charles & King 1998) using the peak luminosity estimate from the *Chandra* observation ($\sim 5\times10^{39}$ erg s^{-1}), the upper limit for the e-fold time (39 days), the accretion efficiency ($\sim$0.1 for an alpha disc: Shakura & Sunyaev 1973) and the critical density for the disc to give an upper limit for the size scale. This gives a radius of 2.6×10^{11} cm and a lower limit for the period of the binary orbit (from Frank, King & Raine 2002) of $>$32.8 hours. In terms of binary parameters and inferred luminosity, this system is then qualitatively similar to 4U 1543-47 (Chen et al. 1997), reinforcing our identification of the system as a LMXB. For a low mass star to fill its Roche lobe in such a wide binary means that the companion is probably somewhat nuclear evolved, i.e. a sub-giant.

The sequence of spectra during the decline can be very roughly described by a standard disc model i.e. inner radius fixed at the innermost stable circular orbit, around a stellar mass ($\sim$10 M$_\odot$) BH. If this is the correct interpretation then, for the first time, we are observing a disc in the Eddington-regime without the hindrance of a large neutral Galactic column, typical of XRBs in our Galaxy. However, this gives residuals of order 10% at low and high energies. This could indicate that even our best disc models are incomplete, e.g. they do not include advection or release of advected radiation from the plunging region or self–shielding (Sądowski 2009; Sądowski et al. 2009). However, these should all give an increasing distortion of the disc spectrum at Eddington and beyond, yet the residuals are seen at a similar or even greater extent in the lowest Eddington fraction spectrum as well as in the highest ones. If this is the correct interpretation of the spectra then our best current disc models can only describe the data within 10% over this wide bandpass. New disc models that fully incorporate the effects of advection, relativistic smearing and energy transport will identify, in a more physically robust manner, how current disc models fail to describe the emission. This dataset will therefore

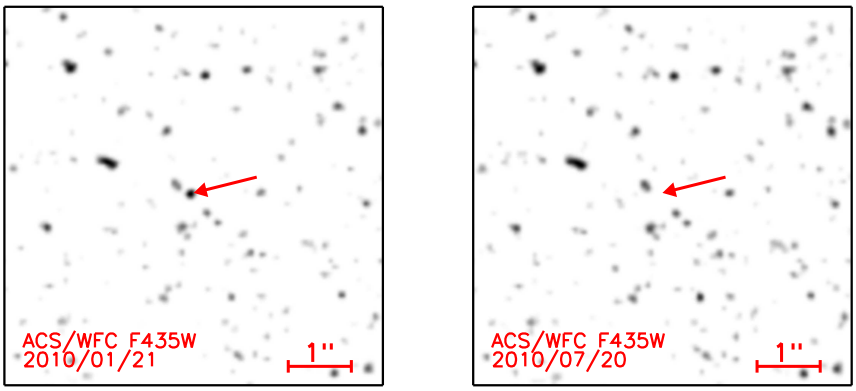


Figure 6. HST (ACS) images taken on the 21st of Jan 2010 (left, OBSID: JB9D15010, PropID=11833) and 20th of July 2010 (right, OBSID: JB9D20010, PropID=11833) for exposures of 4360 s each. The highlighted position is that given in the finding charts of Garcia et al. (2010, ATEL #2474) and, whilst the former observation corresponds to an apparent optical magnitude of 23.8 we determine the latter, quiescent observation to be far fainter: $m_{\rm F435W} \gtrsim 26$. Using the Galactic line-of-sight extinction (Predehl & Schmitt 1995), we derive an upper limit on the absolute magnitude of the optical counterpart in quiescence of $M_{\rm F435W} \approx +1$, ruling out a high mass O or B star companion to the compact object.

prove an invaluable measure of these future models' success (Straub et al. in prep).

Alternatively, the spectra are statistically better fit by an advective (slim) disc model, together with a low temperature, optically thick Comptonisation component which could be the photosphere of an inner-disc wind (e.g. Middleton et al. 2011b). The observed decrease in extent of this wind/photosphere as the luminosity decreases is then due to the reduction in mass loss rate into the wind, so that its photosphere covers less of the inner disc. The observed energy-dependent variability (weakly) supports this two component model, but we caution that this is close to the statistical limit of what the variability data can probe.

We note that the situation remains partially degenerate in terms of spectral components and viewing angles. We would obtain similar fit statistics if the cool component was in fact an outer photosphere and the hot region a modified 'bare' disc where any loose material has already been uplifted and removed in a wind. This is our proposed model for NGC 5408 X-1 (Middleton et al. 2011a) and could likewise predict the same presence of uncorrelated variability via extrinsic means but at a different viewing angle. Whilst this is a much more likely solution for the higher luminosity ULXs, we are currently unable to break this degeneracy in lower luminosity ULXs such as this (and M33 X-8; although that particular source has no constrained variability: Middleton et al. 2011b). In either case, we require a two component solution comprising a wind/photosphere and modified disc emission.

Hence we have a transient system that displays an extraordinary combination of ULX-like luminosities, an e-fold time and derived binary system parameters, and optical counterpart consistent with a classical LMXB transient, and super-Eddington outburst behaviour similar to other ULXs. Additionally, the presence of an IMBH is rejected on the basis of the X-ray characteristics, firmly demonstrating that an IMBH is not necessary to reach ULX luminosities. First and foremost, this then provides a solid evidential link between accretion onto an apparent stellar mass black hole binary and ULX-like behaviour. This evidence exceeds that from previous analyses where the success of super-Eddington emission models lead to the inference of an underlying stellar-mass black hole (e.g. Gladstone et al. 2009); in this case the transience allows far stronger physical links to be made.

However, the transient nature of this object also marks it out as an unusual ULX. Although it has long been known that ULXs are associated with both old and young stellar populations (Humphrey et al. 2003; Colbert et al. 2004), the majority of work has focused on the objects directly linked to young stellar populations as they are both more numerous and more luminous than the older population (cf. Walton et al. 2011). These objects are also typically persistently luminous, unlike the transient discussed here; in fact few transient ULXs have been observed, with notable cases associated with the old population of Cen A (Ghosh et al. 2006; Sivakoff et al. 2008) and a recurrent transient in the outer regions of the archetypal nuclear starburst galaxy NGC 253 (Bauer & Pietsch 2005). However, despite the likely differences in donor star and outburst timescales, the similarity in X-ray spectral characteristics between M31 ULX-1 and other well-studied low luminosity ULXs (e.g. M33 X-8, Middleton et al. 2011b) argues for a commonality in accretion physics and an underlying black hole mass in the stellar regime in many ULXs.

6 ACKNOWLEDGEMENTS

The authors thank the anonymous referee for their useful comments. MM, TR and CD thank STFC for support in the form of a standard grant, and AS similarly thanks STFC for support via a PhD studentship. This work is based on observations obtained with *XMM-Newton*, an ESA science mission with instruments and contributions directly funded by ESA Member States and NASA. We also acknowledge use of archival *Chandra* and *Swift* data. Additionally this work has made use of observations made with the NASA/ESA Hubble Space Telescope, obtained from the data archive at the Space Telescope Institute. STScI is operated by the asso-

ciation of Universities for Research in Astronomy, Inc. under the NASA contract NAS 5-26555

REFERENCES

Abramowicz M. A., Czerny B., Lasota J. P., Szuszkiewicz E., 1988, ApJ, 332, 646
Bauer M., Pietsch W., 2005, A&A, 442, 925
Chen W., Shrader C. R., Livio M., 1997, ApJ, 491, 312
Colbert E. J. M., Heckman T. M., Ptak A. F., Strickland D. K., Weaver K. A., 2004, ApJ, 602, 231
Colbert E. J. M., Mushotzky R. F., 1999, ApJ, 519,
Czerny B., Hryniewicz K., Nikołajuk M., Sądowski A., 2011, MNRAS, 415, 2942
Davis S. W., Blaes O. M., Hubeny I., Turner N. J., 2005, ApJ, 621, 372
Dickey J. M., Lockman F. J., 1990, ARA&A, 28, 215
Done C., Gierliński M., 2003, MNRAS, 342, 1041
Done C., Davis S., Jin C., Blaes O., Ward M., 2011, arXiv, arXiv:1107.5429
Done C., Gierliński M., Kubota A., 2007, A&ARv, 15, 1
Dubus G., Charles P. A., Long K. S., 2004, A&A, 425, 95
Edelson R., Turner T. J., Pounds K., Vaughan S., Markowitz A., Marshall H., Dobbie P., Warwick R., 2002, ApJ, 568, 610
Frank J., King A., Raine D. J., 2002, apa..book,
Ghosh K. K., Finger M. H., Swartz D. A., Tennant A. F., Wu K., 2006, ApJ, 640, 459
Gladstone J. C., Roberts T. P., Done C., 2009, MNRAS, 397, 1836
Henze M., Pietsch W., Haberl F., Greiner J., 2009, ATel, 2356, 1
Humphrey P. J., Fabbiano G., Elvis M., Church M. J., Bałucińska-Church M., 2003, MNRAS, 344, 134
Kajava J. J. E., Poutanen J., 2009, MNRAS, 398, 1450
Kaur A., et al., 2011, arXiv:1109.1547
King A. R., 1999, PhR, 311, 337
King A. R., 2004, NuPhS, 132, 376
Kolehmainen M., Done C., Díaz Trigo M., 2011, MNRAS, 416, 311
Kubota A., Makishima K., Ebisawa K., 2001, ApJ, 560, L147
Kubota A., Done C., Davis S. W., Dotani T., Mizuno T., Ueda Y., 2010, ApJ, 714, 860
La Parola V., Damiani F., Fabbiano G., Peres G., 2003, ApJ, 583, 758
McClintock J. E., Remillard R. A., 2006, csxs.book, 157
Middleton M. J., Roberts T. P., Done C., Jackson F. E., 2011, MNRAS, 411, 644
Middleton M. J., Sutton A. D., Roberts T. P., 2011, MNRAS, 417, 464
Mineshige S., Kawaguchi T., Takeuchi M., Hayashida K., 2000, PASJ, 52, 499
Mineshige S., Yamasaki T., Ishizaka C., 1993, PASJ, 45, 707
Ohsuga K., 2007, ApJ, 659, 205
Ohsuga K., Mineshige S., 2011, ApJ, 736, 2
Ohsuga K., Mineshige S., Mori M., Kato Y., 2009, PASJ, 61, L7
Orosz J. A., McClintock J. E., Remillard R. A., Corbel S., 2004, ApJ, 616, 376
Pietsch W., et al., 2009, ApJ, 694, 449
Parmar A. N., et al., 2001, A&A, 368, 420
Poutanen J., Lipunova G., Fabrika S., Butkevich A. G., Abolmasov P., 2007, MNRAS, 377, 1187
Predehl P., Schmitt J. H. M. M., 1995, A&A, 293, 889
Revnivtsev M., Gilfanov M., Churazov E., Sunyaev R., 2002, A&A, 391, 1013
Roberts T. P., 2007, Ap&SS, 311, 203
Sądowski A., 2009, ApJS, 183, 171
Sadowski A., Abramowicz M. A., Bursa M., Kluźniak W., Różańska A., Straub O., 2009, A&A, 502, 7
Shahbaz T., Charles P. A., King A. R., 1998, MNRAS, 301, 382
Shakura N. I., Sunyaev R. A., 1973, A&A, 24, 337
Sivakoff G. R., et al., 2008, ApJ, 677, L27
Steiner J. F., Narayan R., McClintock J. E., Ebisawa K., 2009, PASP, 121, 1279
Takano M., Mitsuda K., Fukazawa Y., Nagase F., 1994, ApJ, 436, L47
Tanaka M., Chiba M., Komiyama Y., Guhathakurta P., Kalirai J. S., Iye M., 2010, ApJ, 708, 1168
Titarchuk L., 1994, ApJ, 434, 570
van Paradijs J., 1996, ApJ, 464, L139
Vaughan S., Edelson R., Warwick R. S., Uttley P., 2003, MNRAS, 345, 1271
Vilardell F., Ribas I., Jordi C., Fitzpatrick E. L., Guinan E. F., 2010, A&A, 509, A70
Walton D. J., Roberts T. P., Mateos S., Heard V., 2011, MNRAS, 1147
Warwick R. S., Pérez-Ramírez D., Byckling K., 2011, MNRAS, 413, 595
Weng S.-S., Wang J.-X., Gu W.-M., Lu J.-F., 2009, PASJ, 61, 1287
Wilkinson T., Uttley P., 2009, MNRAS, 397, 666
Życki P. T., Done C., Smith D. A., 1999, MNRAS, 309, 561